ELSEVIER

Journal of Wind Engineering
and Industrial Aerodynamics 81 (1999) 283–293

JOURNAL OF wind engineering AND industrial aerodynamics

Numerical simulation of atmospheric flow over complex terrain

Takanori Uchida[a,*], Yuji Ohya[b]

[a]*Interdisciplinary Graduate School of Engineering Sciences, Kyushu University, Kasuga-shi 816-8580, Japan*
[b]*Research Institute for Applied Mechanics, Kyushu University, Kasuga-shi 816-8580, Japan*

Abstract

In order to develop an overall efficient and accurate method of simulating an unsteady three-dimensional atmospheric flow over topography, we examined two grid systems and corresponding variable arrangements: one is a body-fitted coordinate (BFC) grid system based on a collocated variable arrangement; the other is an orthogonal grid system based on a staggered variable arrangement. Using these codes, we calculated the wind system over topography such as an isolated hill and real complex terrain. Both codes remarkably removed the numerical difficulties such as the convergence of the SOR method in solving the pressure Poisson equation, resulting in numerical results with much higher accuracy. Despite the differences in the grid system and in variable arrangement, no significant differences in the flow pattern between the both numerical results were found. Compared with the previous studies, the numerical results obtained are very satisfactory in the sense that overall characteristic flows are successfully simulated irrespective of the simulation codes.

Keywords: Computational fluid dynamics; Finite-difference method; Body-fitted coordinate (BFC) grid system; Collocated variable arrangement; Orthogonal grid system; Staggered variable arrangement; Isolated hill; Real complex terrain

1. Introduction

Atmospheric phenomena span a huge range of scales in both space and time, and have a strong dependence on a variety of meteorological elements such as turbulence,

* Corresponding author.
E-mail address: takanori@riam.kyushu-u.ac.jp (T. Uchida)

0167-6105/99/$ - see front matter
PII: S0167-6105(99)00024-0

buoyancy, topographic effect and rotation of the Earth. Understanding and predicting the regional distribution of meteorological variables (e.g., wind, temperature, humidity, radiation budget, turbulent kinetic energy) of these phenomena are quite necessary because they have strong relationships with industrial planning and environmental problems.

Now a days we have four major tools to investigate the atmospheric phenomena: (1) field study; (2) theoretical study; (3) experimental study; (4) numerical study. Most theoretical studies that have been done to date are restricted to two-dimensional flows. Both experimental and field studies are usually expensive, and often provide data that is not sufficiently detailed. On the other hand, a numerical study (often called a computational fluid dynamics, CFD) has become indeed one of the most useful tools for studying the atmospheric phenomena in recent years mainly due to the increasing power of the new generations of computers. However, it is still hard and time consuming to make a three-dimensional computation of an unsteady atmospheric flow over topography.

Therefore, we have developed a couple of efficient simulation codes using a finite-difference method (hereafter FDM) from a wind engineering point of view [1–6]. These simulation codes are based on a direct numerical simulation (hereafter DNS) [1–4], which involves the numerical solution of the Navier–Stokes equation without any turbulent model, and are based on a large eddy simulation (hereafter LES) as a turbulent model [5,6], which means that only large eddies of fluid motion are simulated explicitly while those smaller than the grid size are modeled by a dynamic subgrid-scale model [7].

The present numerical study described here follows on from the previous numerical studies mentioned above [1–6]. The basic objective of this study is to develop an overall efficient and accurate method of simulating an unsteady three-dimensional atmospheric flow over topography with characteristic length scales of the order of kilometers and characteristic time scales of the order of hours. For this purpose, we examine two grid systems and corresponding variable arrangements.

First, we investigate stably stratified atmospheric flows over an isolated hill as a simple terrain by using these codes. Attention is focused on the efficiency, accuracy and applicability of these codes. Stably stratified atmospheric flows over topography have attracted great interest from not only fluid mechanicians but also engineers in a variety of fields. Investigations of pollutant transport and dispersion in stably stratified atmospheric flows over complex relief are critical for the protection of air quality, because industrial plants and other sources of air pollution are frequently located within or near complex terrain. The stable stratification effects strongly influence plume behaviors over complex terrain. Depending on the release height and the stratified conditions, plumes may be observed to be entrained into rotors or vortices of numerous types, or to be transported long distances with little or no dispersion.

Next, we consider the calculation of a non-stratified atmospheric flow (i.e., neutral flow) over real complex terrain in a horizontal region of 25 km $\times$ 25 km with a relatively fine spatial resolution. Particular emphasis is placed on whether the wind system observed in the previous wind tunnel experiment [8] can be successfully simulated by using these codes.

2. Numerical model

2.1. Governing equations

We consider a linearly density stratified flow of incompressible and viscous fluid over three-dimensional topography such as an isolated hill and complex terrain in a domain with infinite upper boundary. In an attempt to compare the numerical results with the previous experimental [1–3,8,9] and numerical [10] results, the Coriolis force is neglected. Under the Boussinesq approximation, the dimensional governing equations for unknown variables $u_i = (u, v, w)$, ρ' and p' used in this study consist of the continuity, Navier–Stokes and density equations as follows:

$$\frac{\partial u_i}{\partial x_i} = 0, \tag{1}$$

$$\frac{\partial u_i}{\partial t} + u_j \frac{\partial u_i}{\partial x_j} = -\frac{1}{\rho_0}\frac{\partial p'}{\partial x_i} + \frac{\mu}{\rho_0}\frac{\partial^2 u_i}{\partial x_j \partial x_j} - \frac{\rho' g \delta_{i\,3}}{\rho_0}, \tag{2}$$

$$\frac{\partial \rho'}{\partial t} + u_j \frac{\partial \rho'}{\partial x_j} = \alpha \frac{\partial^2 \rho'}{\partial x_j \partial x_j} - w\frac{\mathrm{d}\rho_B}{\mathrm{d}z}, \tag{3}$$

ρ' and p' are the perturbation density and pressure defined as

$$\rho' = \rho - \rho_B(z), \quad p' = p - p_B(z), \tag{4}$$

where $x_i = (x, y, z)$ are the physical coordinate components, $u_i = (u, v, w)$ are the corresponding velocity components, ρ_0 is the reference density, μ is the viscosity coefficient, g is the acceleration due to gravity and α is the molecular diffusivity for density. $\rho_B(z)$ and $p_B(z)$, which satisfy the hydrostatic equilibrium $\mathrm{d}p_B(z)/\mathrm{d}z = -\rho_B(z)g$, are the undisturbed basic distributions at the inflow boundary and $\rho_B(z)$ decreases linearly with height, namely, $\mathrm{d}\rho_B(z)/\mathrm{d}z = -1$. The subscripts i, j, k take values of 1, 2, 3 to denote the streamwise (x), spanwise (y) and vertical (z) directions, respectively. Non-dimensionalizing all variables using the uniform upstream velocity U, topography height h and reference density ρ_0, we have three dimensionless equations as follows:

$$\frac{\partial u_i}{\partial x_i} = 0, \tag{5}$$

$$\frac{\partial u_i}{\partial t} + u_j \frac{\partial u_i}{\partial x_j} = \frac{\partial p}{\partial x_i} + \frac{1}{\mathrm{Re}}\frac{\partial^2 u_i}{\partial x_j \partial x_j} - \frac{\rho \delta_{i3}}{Fr^2}, \tag{6}$$

$$\frac{\partial \rho}{\partial t} + u_j \frac{\partial \rho}{\partial x_j} = \frac{1}{\mathrm{RePr}}\frac{\partial^2 \rho}{\partial x_j \partial x_j} + w. \tag{7}$$

These governing equations include three dimensionless parameters, i.e., the Reynolds number Re ($=\rho_0 Uh/\mu$), Prandtl number Pr ($=\mu/\alpha\rho_0$) and Froude number Fr ($=U/Nh$), where N is the buoyancy frequency defined as $N^2 = -(g/\rho_0)(\mathrm{d}\rho_B/\mathrm{d}z)$.

2.2. Numerical simulation method

The numerical method is as follows. The coupling algorithm of the velocity components and pressure is a fractional step method [11], therefore, the distribution of pressure is determined by solving the Poisson equation, derived by taking divergence of Eq. (6), using the successive over relaxation (hereafter SOR) method. The Euler explicit method with a first-order accuracy is used for time advancement in Eq. (6) and Eq. (7). As for the discretization of spatial derivatives in the governing equations, we employ a second-order central scheme except for advective terms. For advective terms which are non-conservation form, a third-order upwind scheme [10] is employed. Accordingly, the present numerical method is based on a pseudo-direct simulation [12].

2.3. Grid system

The most important factor to the success of the numerical simulation of the atmospheric flow over three-dimensional topography is how to specify the topography model as the boundary condition in the computation. For this purpose, we examine two grid systems and corresponding variable arrangements, as shown in Figs. 1 and 2: one is a body-fitted coordinate (hereafter BFC) grid system in Fig. 1(a); the other is an orthogonal grid system in Fig. 1(b). Note that in the latter case, the topography model is approximated by rectangular grids.

If we employ a BFC grid system, then the original governing equations (Eqs. (5)–(7)) in the physical space are transformed to the computational space through a coordinate transformation ($x = x(\xi, \eta, \zeta), y = y(\xi, \eta, \zeta), z = z(\xi, \eta, \zeta)$) and their equations are

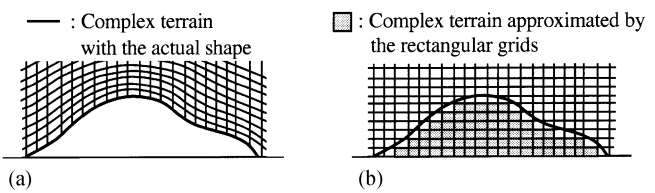

Fig. 1. Grid system: (a) BFC grid system; (b) orthogonal grid system.

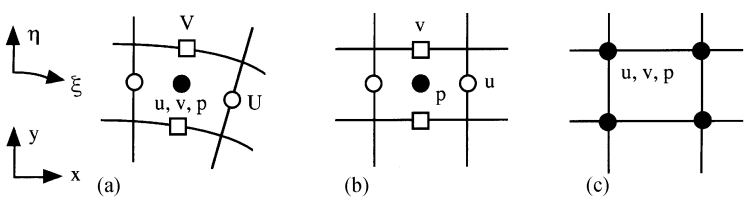

Fig. 2. Variable arrangement. Notations are (x, y): physical coordinate components; (ξ, η): BFC components; (u, v): Cartesian velocity components; (U, V): volume flux components; (p): pressure; (a) collocated grid; (b) staggered grid; (c) regular grid.

approximated by a FDM based on a collocated grid [13] where the Cartesian velocity components and pressure are defined at the center of a cell, while the volume flux components are defined at the mid-point on their corresponding cell surfaces, as shown in Fig. 2(a) [hereafter code I].

On the other hand, if we employ an orthogonal grid system, then without any coordinate transformation, the original governing equations (Eqs. (5)–(7)) in the physical space are directly approximated by a FDM based on a non-uniform staggered grid [11] where the Cartesian velocity components are defined at the mid-point on their corresponding cell surfaces, while only the pressure is defined at the center of a cell, as shown in Fig. 2(b) [hereafter code II]. As a result, for the computations using an orthogonal grid system, the governing equations approximated by a FDM become simpler than those based on a BFC grid system.

In the previous numerical studies [1–3], irrespective of grid systems in Fig. 1, we employed a regular grid where all variables are defined at the same location, as shown in Fig. 2(c) [hereafter code III]. Then, we experienced non-physical numerical oscillations, which always appeared when the grid resolution was not sufficient, and an inefficient convergence of the SOR method for solving the pressure Poisson equation. Therefore, in order to evaluate the performance of code I and code II in terms of phenomena aforementioned, we conducted preliminary computations with the same parameters used in the previous numerical studies [1–3] (e.g., the grid resolution, Reynolds number, Froude number and non-dimensional time step). Consequently, both cases showed no numerical oscillations in the results, and brought a considerable improvement over the code III for the convergence of the SOR method in solving the pressure Poisson equation.

3. Numerical results

3.1. Stably stratified atmospheric flows over an isolated hill

In order to test the efficiency, accuracy and applicability of code I and code II, we calculate stably stratified atmospheric flows over an isolated hill as a simple terrain with a moderate slope under various Froude numbers. The computational domain consists of a streamwise length $L_x = 16.5h$, spanwise length $L_y = 10h$ and vertical length $L_z = 5h$, where h is the height of the hill. An isolated hill is placed at the center in the spanwise direction and the center of the hill is a distance of $4.5h$ from the inflow boundary. The shape of an isolated hill is defined as $f(r) = h/(1 + r^4)$, where $f(r)$ is the height and r is the distance from the center of the hill. For both cases, the number of grid points is $111 \times 61 \times 51$ in the x-, y- and z-directions, respectively and the vertical smallest grid spacing at the top of the hill is approximately $1.5 \times 10^{-3}h$. To identify the change in the flow pattern with various Froude numbers, we calculate the cases of $\mathrm{Fr} = \infty$ (neutral flow), 1, 0.1 at a Reynolds number $\mathrm{Re} = 5 \times 10^3$, based on the uniform upstream velocity U and hill height h, and Prandtl number $\mathrm{Pr} = 0.71$ (air). We employ an impulsive-start as initial condition. The boundary conditions are as follows: for velocity, $U = 1$ (inflow), Sommerfeld radiation condition (outflow),

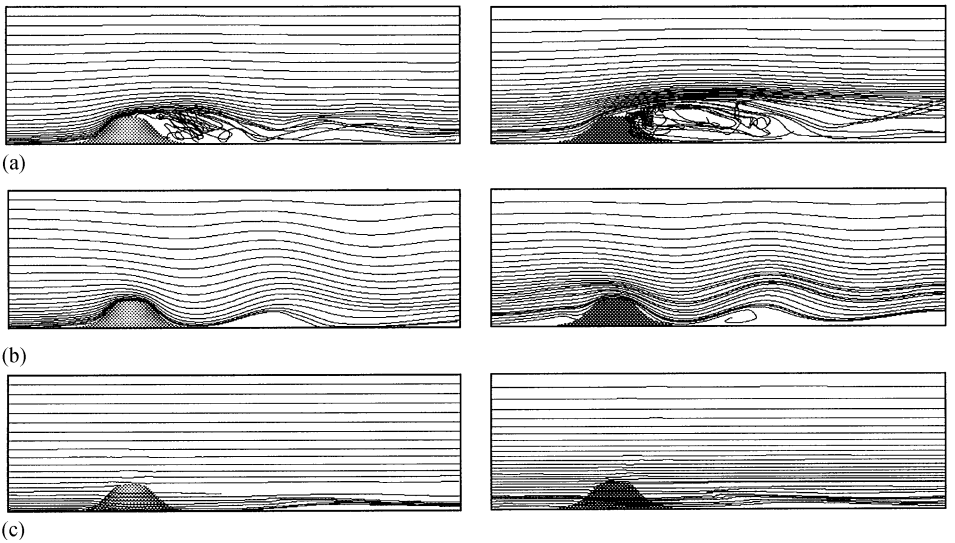

Fig. 3. Instantaneous streamlines in the vertical plane passing the top of the hill at a fully developed state ($Re = 5 \times 10^3$): (left) BFC grid system; (right) orthogonal grid system. Flow is left to right; (a) Neutral flow ($Fr = \infty$); (b) stably stratified flow ($Fr = 1$); (c) stably stratified flow ($Fr = 0.1$).

free-slip condition (top and side boundaries), no-slip condition (ground and topography): for pressure, Neumann condition (all boundaries): for density, zero (inflow), free-slip condition (all other boundaries). The non-dimensional time step is around $\Delta t = (1\text{–}2) \times 10^{-3}$.

Fig. 3 shows the instantaneous streamlines in the vertical plane passing the top of the hill at a fully developed state. A coherent structure of eddies in the lee of the hill is confirmed at a Froude number $Fr = \infty$ (neutral flow) in Fig. 3(a). Note that these eddies form quasi-periodic vortex shedding from the hill. For the cases of $Fr = 1$ and 0.1, the flow field around the hill is dramatically altered by addition of stable stratification. At a Froude number $Fr = 1$ in Fig. 3(b), a lee wave with long wavelength is excited downstream of the hill. This lee wave strongly affects the unsteady separated and reattaching flow behind the hill, resulting in that fluid flows along the lee slope without separation. The upward flow in the first lee wave motion induces a rotor under the crest of the lee wave. According to the linear theory, the wavelength of the lee wave is predicted by $\lambda/h = 2\pi U/(Nh) = 2\pi Fr$ independent of the hill shape. The values obtained by the present calculation at $Fr = 1$ in Fig. 3(b) are consistent with the prediction of the linear theory (note that the wavelength was calculated from the first lee wave depicted by the instantaneous streamlines in Fig. 3(b) because the wave amplitude decayed rapidly). At a Froude number $Fr = 0.1$ in Fig. 3(c), the vertical fluid motion is severely suppressed. The flow separates just when it passes the top of the hill. Most fluids rather go around the sides of the hill horizontally than go over the top of it. For strongly stratified flow over topography (i.e., when the Froude number $Fr < 1$), it is well known that the dividing streamline

height H_s, defined as $H_s/h = 1 - \mathrm{Fr}$, is a simple criterion regarding the fluid parcel behavior. This formula was derived by Hunt et al. [9] from Sheppard's formula [14] under the conditions of uniform upstream velocity and linear stratification, and can be physically interpreted as follows: if the fluid parcel upstream the topography is originally located at a higher level than H_s, then it goes over the top of the topography and the remaining fluid parcel may move the sides of it horizontally. In other words, the dividing streamline height H_s forms the boundary between a lower layer of essentially horizontal flow and an upper layer that passes over the hilltop. In Fig. 3(c), we confirmed the existence of the dividing streamline and its value H_s is in good agreement with the one predicted.

As the Froude number becomes sufficiently small, the fluid parcel upwind the hill impinges on the hill surface, splits and travels around the sides of the hill horizontally, as shown in Fig. 3(c). Therefore, to investigate the horizontal flow field in the lower layer in more detail at $\mathrm{Fr} = 0.1$, we examined the time evolution of streamlines in the horizontal plane at a height of $0.4h$ above ground and these figures are shown in Fig. 4. A pair of vortices behind the hill can be clearly seen at $t = 10$ in Fig. 4(a). As time proceeds, the instability in a pair of vortices behind the hill becomes gradually dominant at $t = 30$ in Fig. 4(b) and then vortices behind the hill are almost periodically shed downstream of the hill at $t = 100$ in Fig. 4(c) as like the familiar Karman vortex street observed downwind of two-dimensional cylinders in neutral flow.

This example clearly demonstrated several improvements in the efficiency, accuracy and applicability to stably stratified atmospheric flows under stable stratification as follows. First, both cases remarkably removed the numerical difficulties inherent to stably stratified atmospheric flows, and brought results with much higher accuracy. Secondly, despite of the differences in the grid system (i.e., BFC and orthogonal grid) and in the variable arrangement (i.e., collocated and staggered variable arrangement), no significant differences in both numerical results obtained by codes I and II were found. As it is expected, the code II was more efficient than the code I for CPU time and memory usage. Thirdly, compared with the theoretical, experimental [1–3,9] and numerical [10] results (not shown here), good agreement was obtained in the characteristic phenomena of stably stratified atmospheric flows over an isolated hill with a variety of Froude numbers.

3.2. A non-stratified atmospheric flow over real complex terrain

Using codes I and II, we consider the calculation of a non-stratified flow (neutral flow) over real complex terrain.

Fig. 5 shows a perspective view of the computational domain which covers the northern part of Kyushu in Japan, including Mt. Adachi (598 m) in the north, Mt. Nuki (717 m) in the south and the Suo Nada (sea) in the east. The computational domain has a height of 5 km in the z-direction and both streamwise and spanwise lengths of 25 km in the x- and y-directions.

In order to consider the significant details of complex terrain, we overlaid horizontal grids with an equal size of Δx and $\Delta y = 250$ m in the x- and y-directions and vertical non-uniform grids in the z-direction, concentrated toward the ground, over

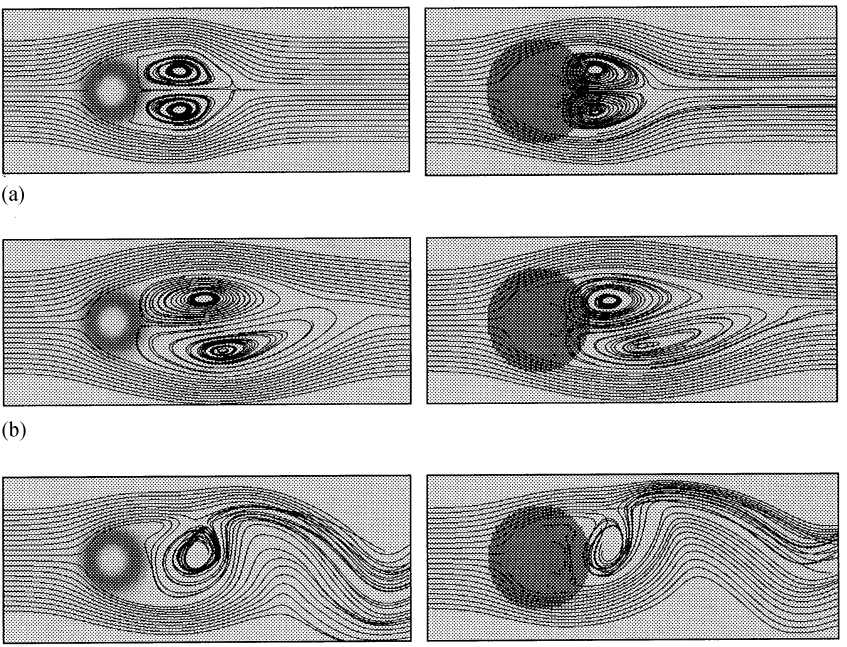

Fig. 4. Time evolution of streamlines in the horizontal plane at a height of 0.4 h above ground (Fr = 0.1, $Re = 5 \times 10^3$): (left) BFC grid system; (right) orthogonal grid system. Flow is left to right; (a) $t = 10$; (b) $t = 30$; (c) $t = 100$.

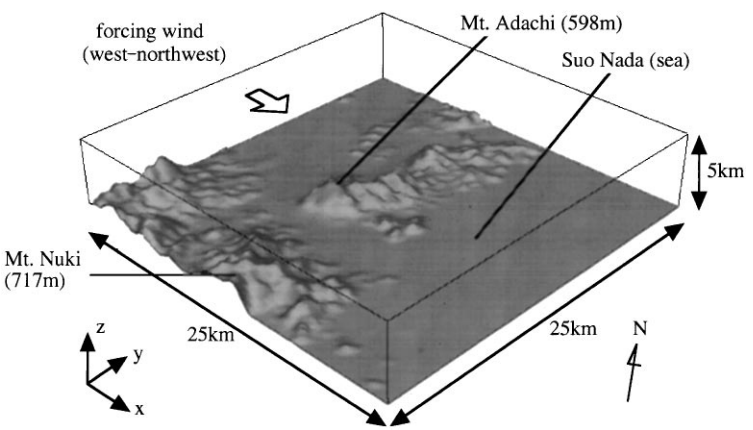

Fig. 5. Perspective view of the computational domain.

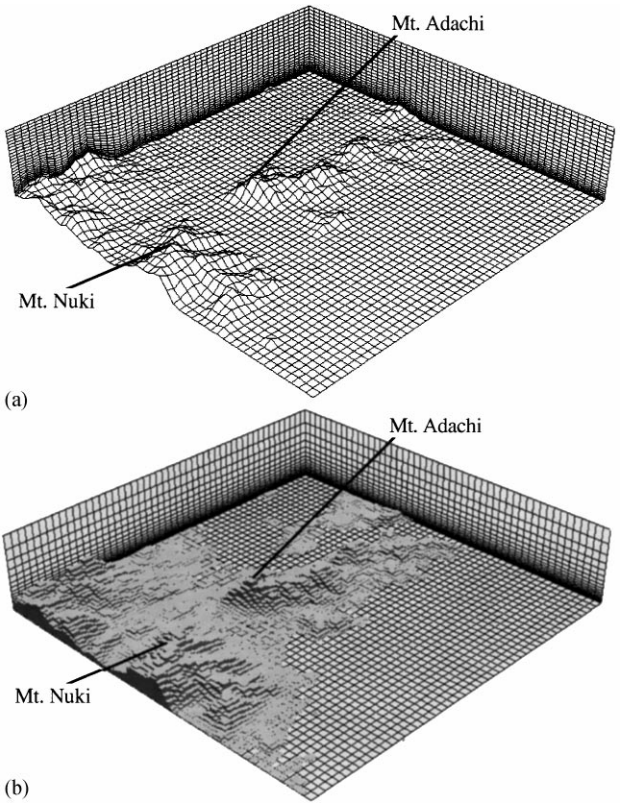

Fig. 6. Grid system. (a) BFC grid system; (b) orthogonal grid system.

the computational domain for both cases, as shown in Fig. 6. Minimum size of Δz is approximately 5 m for both cases. The number of grid points in the x-, y- and z-directions is $101 \times 101 \times 51$ for both cases. The altitudes of the topography are based on a digital data tape (KS-110-1) provided by the Japan Map Center. We specify the west-northwest wind as the forcing wind as well as the previous wind tunnel experiment [8]. The boundary conditions are as follows: for velocity, $U = 1$ (inflow), Sommerfeld radiation condition (outflow), free-slip condition (top and side boundaries), no-slip condition (ground and topography): for pressure, Neumann condition (all boundaries). The Reynolds number, based on the uniform upstream velocity U (west-northwest wind) and height h of Mt. Adachi (598 m), is set at 10^4 corresponding to the previous wind tunnel experiment [8].

Fig. 7 shows the instantaneous streamlines near the ground at a fully developed state. From flow visualization using a smoke wire technique [8], we have obtained the following characteristic features regarding the wind system over this region: (1) there exists a coherent structure of eddies in the lee of Mt. Adachi, which forms quasi-periodic vortex shedding from Mt. Adachi; (2) converged and accelerated flows

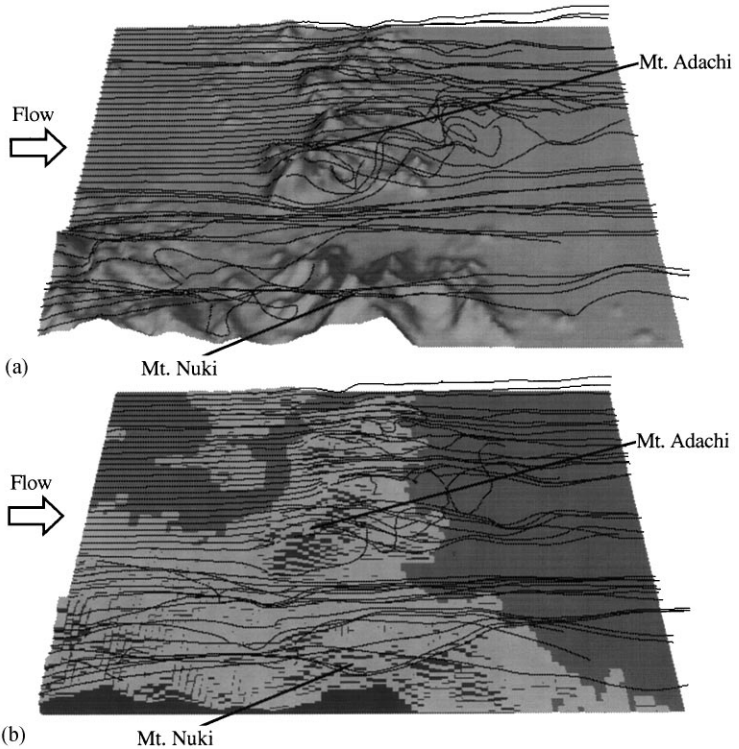

Fig. 7. Instantaneous streamlines near the ground at a fully developed state ($Fr = \infty$, $Re = 10^4$): (a) BFC grid sytem; (b) orthogonal grid system.

between Mt. Adachi and Mt. Nuki are clearly found and flow going around the sides of Mt. Adachi and Mt. Nuki is also confirmed. From Fig. 7, we can see that qualitative features aforementioned are successfully simulated in the numerical results irrespective of the simulation codes. In addition, we can notice that the surface winds are strongly influenced by the topographic effects for both cases. The numerical results with stably stratified flows can be found in Ref. [4].

4. Concluding remarks

In order to develop an overall efficient and accurate method of simulating an unsteady three-dimensional atmospheric flow over topography, which is based on a FDM, we examined two grid systems and corresponding variable arrangements: one is a BFC grid system based on a collocated variable arrangement (code I); the other is an orthogonal grid system based on a staggered variable arrangement (code II). In the latter case, the topography model is approximated by rectangular grids. Using these codes, we calculated the wind system over topography such as an

isolated hill and real complex terrain. The numerical results obtained are summarized as follows:

(1) Codes I and II remarkably removed the numerical difficulties such as the convergence of the SOR method in solving the pressure Poisson equation, resulting in numerical results with much higher accuracy, especially for computations with stably stratified atmospheric flows.

(2) Despite the differences in the grid system and in the variable arrangement, no significant differences in the flow pattern between codes I and II were found. As it is expected, the code II was more efficient than the code I for CPU time and memory usage.

(3) Compared with the theoretical, experimental [1–3,8,9] and numerical [10] results, good agreement was obtained in the overall characteristic features of the wind system over topography irrespective of the simulation codes.

Application to stably stratified atmospheric flows with high Reynolds numbers is currently under investigation by using a LES as a turbulent model.

References

[1] T. Uchida, Y. Ohya, S. Ozono, Numerical simulation of stably stratified flows past a 3D complex terrain, Proc. 14th Japan Wind Engineering Symposium 1996, pp. 91–96 (in Japanese).

[2] T. Uchida, Y. Ohya, Numerical simulation of stably stratified flows past a three-dimensional obstacle on the ground, Proc. 10th Japan CFD Symposium 1996, pp. 304–305 (in Japanese).

[3] T. Uchida, Y. Ohya, Wind system prediction of stably stratified flows past a complex terrain – comparison of the rectangular grid system and the generalized curvilinear grid system, Reports of Research Institute for Applied Mechanics, vol. 82, 1997, pp. 113–126 (in Japanese).

[4] T. Uchida, Y. Ohya, Prediction of wind system for stably stratified flows over complex terrain using a generalized curvilinear coordinate system based on a collocated grid, Proc. 15th Japan Wind Engineering Symposium, 1998, pp. 131–136 (in Japanese).

[5] T. Uchida, Y. Ohya, Large eddy simulation of neutral flow past a complex terrain using a dynamic SGS model, Proc. 8th Computation and Fluid Mechanics Symposium 1997, pp. 343–344 (in Japanese).

[6] T. Uchida, Y. Ohya, Large eddy simulation of stably stratified flows past a complex terrain using a dynamic SGS model, Proc. 11th Japan CFD Symposium 1997, pp. 173–174 (in Japanese).

[7] M. Germano, U. Piomelli, P. Moin, W.H. Cobat, A dynamic subgrid-scale eddy viscosity model, Phys. Fluids A 3 (1991) 1760–1765.

[8] S. Ozono, Y. Ohya, Simulation of airflow in a coastal area with complex terrain, Proc. 14th Japan Wind Engineering Symposium, 1996, pp. 85–90.

[9] J.C.R. Hunt, W.H. Snyder, Experiments on stably and neutrally stratified flow over a model three-dimensional hill, J. Fluid Mech. 96 (1980) 671–704.

[10] M. Suzuki, K. Kuwahara, Stratified flow past a bell-shaped hill, Fluid Dyn. Res. 9 (1992) 1–18.

[11] J. Kim, P. Moin, Application of a fractional-step method to incompressible Navier–Stokes equations, J. Comput. Phys. 59 (1985) 308–323.

[12] M. Lesieur, O. Metais, New trends in large-eddy simulations of turbulence, Ann. Rev. Fluid Mech. 28 (1996) 45–82.

[13] Y. Zang, R.L. Street, J.R. Koseff, A non-staggered grid, fractional step method for time-dependent incompressible Navier–Stokes equations in curvilinear coordinates, J. Comput. Phys. 114 (1994) 18–33.

[14] P.A. Sheppard, Airflow over mountains, Quart. J. Roy. Met. Soc. 82 (1956) 528–529.